Complete fusion of ^{9}Be with spherical targets

Henning Esbensen*
Physics Division, Argonne National Laboratory, Argonne, Illinois 60439, USA
(Received 12 February 2010; published 17 March 2010)

The complete fusion of ^{9}Be with ^{144}Sm and ^{208}Pb targets is calculated in the coupled-channels approach. The calculations include couplings among the $3/2^-$, $5/2^-$, and $7/2^-$ states in the $K = 3/2$ ground-state rotational band of ^{9}Be. It is shown that the $B(E2)$ values for the excitation of these states are accurately described in the rotor model. The interaction of the strongly deformed ^{9}Be nucleus with a spherical target is calculated using the double-folding technique and the effective M3Y interaction, which is supplemented with a repulsive term that is adjusted to optimize the fit to the data for the ^{144}Sm target. The complete fusion is described by ingoing-wave boundary conditions. The decay of the unbound excited states in ^{9}Be is considered explicitly in the calculations by using complex excitation energies. The model gives an excellent account of the complete fusion (CF) data for ^{9}Be + ^{144}Sm, and the cross sections for the decay of the excited states are in surprisingly good agreement with the incomplete fusion (ICF) data. Similar calculations for ^{9}Be + ^{208}Pb explain the total fusion data at high energies but fail to explain the CF data, which are suppressed by 20%, and the calculated cross section for the decay of excited states is a factor of 3 smaller than the ICF data at high energies. Possible reasons for these discrepancies are discussed.

DOI: 10.1103/PhysRevC.81.034606 PACS number(s): 25.60.Pj, 24.10.Eq, 25.70.−z

I. INTRODUCTION

The influence of breakup on the complete and incomplete fusion (CF and ICF) of weakly bound nuclei with stable targets is currently being studied at many experimental facilities around the world. Experiments with unstable nuclei are particularly challenging because of weak beam currents and poor statistics. Fortunately, there are several light elements that are both stable and weakly bound and they provide the opportunity to study the influence of breakup on fusion with good statistics.

A good example of a stable and weakly bound nucleus is ^{9}Be, and its fusion has been measured with ^{208}Pb and ^{144}Sm targets [1–3]. The simplest view of ^{9}Be is a strongly deformed three-body system consisting of two α particles held together by a weakly bound neutron. The Q value for the $\alpha + \alpha + n$ three-body breakup is -1.574 MeV. In both experiments it was possible to separate the complete from the ICF.

One of the most dominant features in coupled-channels calculations of fusion of the strongly deformed ^{9}Be nucleus with a stable target is the excitation of states in the $K = 3/2$ ground-state rotational band of ^{9}Be. The large quadrupole deformation of ^{9}Be (derived from the measured quadrupole moment of the ground state) implies that conventional calculations that are based on a deformed Woods-Saxon potential may become unrealistic, for example, if the curvature corrections to the ion-ion potential [4], which are caused by the deformation of the reacting nuclei, are ignored. These problems are overcome in the following by using the double-folding technique [5,6] to calculate the Coulomb plus nuclear interaction between the deformed ^{9}Be nucleus and a spherical target.

Another interesting feature of ^{9}Be is the nonzero spin of the ground state. This feature was pointed out in Ref. [3], and it was recommended that the spin of the $3/2^-$ ground state and the $5/2^-$ and $7/2^-$ excited states of ^{9}Be should be treated explicitly in the calculations. In particular, the fusion cross section should be calculated for each of the initial magnetic quantum numbers, $m = \pm 1/2$ and $m = \pm 3/2$, of the $3/2^-$ ground state of ^{9}Be, and the average cross section should be compared to measurements. In the rotor model one can easily calculate the necessary matrix elements from the multipole expansion of the total interaction between projectile and target.

The structure and parametrization of the one-body density of ^{9}Be are discussed in Sec. II. Calculation of the double-folding interaction between ^{9}Be and a spherical target is presented in Sec. III. A model for calculating the CF cross section is presented in Sec. IV. The results of coupled-channels calculations of the fusion of ^{9}Be + ^{144}Sm and ^{9}Be + ^{208}Pb are presented in Sec. V, and Sec. VI reports the conclusions.

II. STRUCTURE OF ^{9}Be

The nucleus ^{9}Be behaves like an almost-perfect rotor with respect to quadrupole excitations of the $K = 3/2$ ground-state rotational band with spins $I^\pi = 3/2^-$, $5/2^-$, and $7/2^-$. This can be seen by comparing the measured, reduced transition probabilities for quadrupole transitions to the results obtained from Eq. (4.68a) of Ref. [7]:

$$B(E2, KI \rightarrow KI') = \frac{5Q_0^2 e^2}{16\pi} \langle IK20|I'K\rangle^2, \qquad (1)$$

which applies to a perfect rotor. Here Q_0 is the intrinsic quadrupole moment. The measured quadrupole moment of the $3/2^-$ ground state of ^{9}Be is 5.29(4) fm^2 [8], which translates into the intrinsic quadrupole moment $Q_0 = 26.45(20)$ fm^2, according to Eq. (4-69) of Ref. [7]. Inserting this value into Eq. (1), one obtains the reduced transition probabilities that are shown in the last column in Table I. They are in good agreement

*esbensen@phy.anl.gov

TABLE I. Measured reduced transition probabilities $B(E2, 3/2^- \to I^-)$ for exciting the $K = 3/2$ ground-state rotational band of ^{9}Be [8] are compared to predictions of the rotor model. Excitation energies E_I and decay widths Γ_I [9] are also listed.

Spin I^π	E_I (MeV)	Γ_I (keV)	$B(E2)$ (e^2 fm^4)	
			Experiment	Rotor model
$3/2^-$	0	0	14.0(2)	14
$5/2^-$	2.429	0.78	40.7(6)	36
$7/2^-$	6.38	1210	18.9(3)	20
Sum			73.6(11)	70

with the measured values shown in the fourth column in Table I. The sum of the B values is shown in the last row in Table I. The sum is $5Q_0^2e^2/(16\pi)$ in the rotor model, which differs from the experimental value by about 5%.

A great advantage of the rotor model is that it can be applied to calculate the transition matrix elements in cases where they have not been measured, for example, for the transition from $5/2^-$ to $7/2^-$ and the quadrupole moments of the excited states. One can also calculate matrix elements of the total interaction between ^{9}Be and a spherical target from a multipole expansion of this interaction as discussed in Sec. III.

The excitation energies and widths of the three states are shown in the second and third columns in Table I. Note that the width of the $7/2^-$ state is very large, which implies that the state, if excited, may decay by particle emission before fusion with the target takes place. This possibility is investigated in Secs. IV and V.

There are other low-lying states in ^{9}Be but they are not expected to play any significant role in heavy-ion collisions. Thus the spin-orbit partners of the ground-state rotational band, that is, the $1/2^-$, $3/2^-$, and $5/2^-$ states, will be ignored because the spin excitations are weak. The excitation of positive-parity states, starting with the lowest $1/2^+$ state, is also weak and will be ignored.

A. Density parametrization

The densities of the deformed projectile and spherical target nuclei are parametrized by the expression

$$\rho(r, \theta') = C \frac{1 + \cosh(R/a)}{\cosh(r/a) + \cosh(R/a)}, \tag{2}$$

where C is a normalization constant, R is the radius, and a is the diffuseness. The radius of the deformed, axially symmetric projectile depends on the direction with respect to the symmetry axis. It is parametrized as

$$R(\theta') = R_0[1 + \beta_2 Y_{20}(\theta')], \tag{3}$$

where θ' is the angle between the position vector $\mathbf{r}$ and the direction $\mathbf{e}$ of the symmetry axis.

The advantages of the parametrization, Eq. (2), are that it is similar to a Fermi function at larger values of r and it is well behaved as a function of θ' for $r \to 0$, where it approaches an orientation-independent constant. Another advantage of Eq. (2) is the analytic properties it has for spherical nuclei [10]. For example, the Fourier transform is an analytic function, and the expression for the root-mean-square (rms) radius,

$$\langle r^2 \rangle = \tfrac{3}{5}\left[R^2 + \tfrac{7}{3}(a\pi)^2\right], \tag{4}$$

is an exact relation (see the appendix in Ref. [10].) These features are utilized for the spherical target nuclei, ^{144}Sm and ^{208}Pb. The parameters chosen are reported in Table II. They were adjusted so that the measured rms charge radii [11] were reproduced. The parameters for neutron (ν) densities were assumed to be the same as for protons (π), except in the case of ^{208}Pb, where a slightly larger radius is used to accommodate the neutron skin of this nucleus. The adopted skin thickness $\delta_{np} = \langle r^2 \rangle_n^{1/2} - \langle r^2 \rangle_p^{1/2} \approx 0.16(6)$ fm was chosen because it falls in the midst of values predicted by Skyrme Hartree-Fock calculations [12]. Moreover, it is also consistent with the skin thickness $\delta_{np} = 0.16 \pm (0.02)_{\rm stat} \pm (0.04)_{\rm sys}$ fm that has been extracted from antiprotonic ^{208}Pb atoms [13]. The parameters for ^{9}Be are determined in Sec. II C.

TABLE II. Density parameters for ^{9}Be, ^{144}Sm, and ^{208}Pb. Measured rms charge radii [11], listed in the last column, are reproduced, and so is the intrinsic quadrupole moment of ^{9}Be, $Q_0 = 26.45(20)$ fm^2 [8]. The last row lists the adopted neutron (ν) density parameters for ^{208}Pb; the "rms-exp" radius is estimated from Skyrme Hartree-Fock calculations [12].

Nucleus	R (fm)	a (fm)	β_2	$\langle r^2 \rangle^{1/2}$	rms-exp
^{9}Be	2.08	0.375	1.183	2.540	2.52(1)
^{144}Sm	5.829	0.54	0	4.941	4.947(9)
^{208}Pb(π)	6.60	0.546	0	5.500	5.503(2)
^{208}Pb(ν)	6.82	0.546	0	5.66	5.66

B. Multipole expansion of density

The density of the deformed nucleus is expanded on Legendre polynomials,

$$\rho(r, \theta') = \sum_\lambda \rho_\lambda(r)\ P_\lambda[\cos(\theta')], \tag{5}$$

where $\rho_\lambda(r)$ is calculated numerically:

$$\rho_\lambda(r) = \frac{2\lambda + 1}{2} \int_{-1}^{1} dx\ P_\lambda(x)\rho(\mathbf{r}). \tag{6}$$

The multipole expansion of the Fourier transform of the density is

$$\rho(\mathbf{k}) = \sum_\lambda i^{-\lambda}\rho_\lambda(k)\ P_\lambda[\cos(\theta'_k)], \tag{7}$$

where θ'_k is the angle between $\mathbf{k}$ and the direction $\mathbf{e}$ of the symmetry axis, and

$$\rho_\lambda(k) = 4\pi \int_0^\infty dr r^2 \rho_\lambda(r) j_\lambda(kr). \tag{8}$$

The preceding expressions are used in the next section to calculate the double-folding potential. They are also used to calculate the electric multipole moments of the deformed

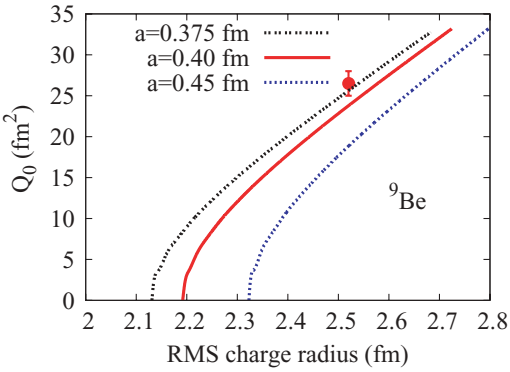

FIG. 1. (Color online) Correlation between the intrinsic quadrupole moment and the rms charge radius of ^{9}Be. Curves were obtained by varying β_2 for the fixed radius parameter $R = 2.08$ and the three values of diffuseness indicated.

charge density $\rho_c(r, \theta')$:

$$M(E\lambda\mu) = M(E\lambda)\, Y_{\lambda\mu}(\mathbf{e}), \tag{9}$$

where

$$M(E\lambda) = \frac{4\pi}{2\lambda+1}\int_0^\infty dr\, r^{\lambda+2}\rho_{c\lambda}(r). \tag{10}$$

The intrinsic quadrupole moment Q_0 is traditionally defined as $2M(E2)$.

C. Calibration of the density of ^{9}Be

The parameters of the density of the deformed ^{9}Be nucleus were adjusted so that both the intrinsic quadrupole moment and the rms charge radius agree with experiments. That was achieved as follows. The mean square charge radius of ^{9}Be,

$$\langle r^2\rangle = \frac{4\pi}{Z}\int_0^\infty dr\, r^4\rho_{c,\lambda=0}(r), \tag{11}$$

and the intrinsic quadrupole moment,

$$Q_0 = 2M(E2) = \frac{4\pi}{5}\int_0^\infty dr\, r^4\rho_{c,\lambda=2}(r), \tag{12}$$

were calculated as functions of the deformation parameter β_2 for a fixed radius $R = 2.08$ fm and for three values of the diffuseness. The results are shown in Fig. 1 as a correlation between the rms charge radius and Q_0. It is shown that the curve that is based on the diffuseness $a = 0.375$ fm passes through the experimental values, and agreement with both values is achieved for $\beta_2 = 1.183$. This is the value that is used in the following, and the shape it produces according to Eq. (3) looks almost like two touching α particles, as illustrated in Fig. 2. In fact, the intrinsic quadrupole moment of ^{9}Be, $Q_0 = 26.45(20)$ fm^2, is almost identical to the calculated quadrupole moment of the unbound nucleus ^{8}Be. The published value obtained in variational Monte Carlo calculations is 26.6(3) fm^2 [14]. The intrinsic quadrupole moment of ^{10}Be is slightly smaller; the value one obtains from the measured $B(E2)$ value of the lowest 2^+ excitation [8] is $Q_0 = 22.9$ fm^2.

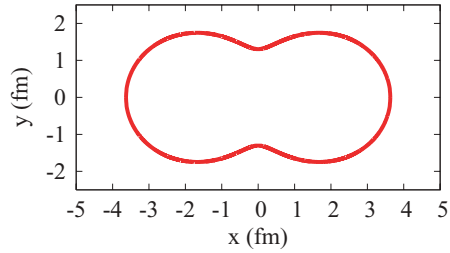

FIG. 2. (Color online) The shape of ^{9}Be, Eq. (3), derived by calibrating the density to reproduce the measured intrinsic quadrupole moment Q_0 and rms charge radius.

III. DOUBLE-FOLDING POTENTIAL

Having adopted the rotor model for ^{9}Be and determined the densities of the projectile and the spherical ^{144}Sm and ^{208}Pb targets, one can now use the double-folding technique to calculate the potential that will be used in the coupled-channels calculations. The double-folding potential is defined by

$$U(\mathbf{r}) = \int d\mathbf{r}_1 \int d\mathbf{r}_2 \rho(\mathbf{r}_1, \mathbf{e})\rho_T(\mathbf{r}_2)v(|\mathbf{r}_2 + \mathbf{r} - \mathbf{r}_1|), \tag{13}$$

where v is the effective nucleon-nucleon interaction and $\mathbf{r}$ is the relative distance between projectile and target. The target density ρ_T is assumed to be spherical, whereas the density of the projectile ^{9}Be is deformed and parametrized as described in the previous section.

The double-folding potential is calculated most conveniently from the Fourier transforms of the densities according to the expression [5]

$$U(\mathbf{r}) = \int \frac{d\mathbf{k}}{(2\pi)^3}\rho(\mathbf{k})\rho_T(-\mathbf{k})v(k)e^{i\mathbf{kr}}. \tag{14}$$

Inserting expression (7) for the deformed projectile and spherical target densities into Eq. (14), one obtains

$$U(\mathbf{r}) = U(r, \theta') = \sum_\lambda U_\lambda(r)P_\lambda[\cos(\theta')], \tag{15}$$

where θ' is the angle between $\mathbf{r}$ and $\mathbf{e}$, and

$$U_\lambda(r) = \frac{1}{2\pi^2}\int dk\, k^2\rho_\lambda(k)\rho_T(k)v(k)j_\lambda(kr). \tag{16}$$

The double-folding calculation of the ion-ion potential and its multipole expansion, Eq. (15), will be based on the M3Y effective interaction, supplemented with a repulsive term that simulates the effect of nuclear incompressibility. This method has been applied previously by Mişicu and Greiner [6] to calculate the fusion between spherical and deformed nuclei. It was also used in Ref. [15] to explain the hindrance in the fusion of spherical nuclei at extreme subbarrier energies.

The repulsive term in the effective NN interaction is parametrized as a contact interaction,

$$v_{NN}^{(\mathrm{rep})}(\mathbf{r}) = v_r\delta(\mathbf{r}), \tag{17}$$

and the densities that are used in the associated double-folding calculation have the same radius as reported in Table I, but usually a much smaller diffuseness a_r is chosen [16]. The value chosen here is $a_r = 0.3$ fm.

The Coulomb interaction can also be generated from Eq. (14) simply by replacing $v(k)$ with the Fourier transform $4\pi e^2/k^2$ of the proton-proton Coulomb interaction and replacing the nuclear densities with the charge densities ρ_c of projectile and target. The result has the same form as Eq. (15):

$$U_C(r,\theta') = \sum_\lambda U_\lambda^C(r) P_\lambda[\cos(\theta')], \tag{18}$$

where

$$U_\lambda^C(r) = \frac{1}{2\pi^2} \int dk\, k^2 \rho_{c,\lambda}(k) \rho_{c,T}(k) \frac{4\pi e^2}{k^2} j_\lambda(kr). \tag{19}$$

For large separations of projectile and target, this interaction approaches the usual monopole-multipole interaction:

$$U_\lambda^C(r) = \frac{Z_T e^2 M(E\lambda)}{r^{\lambda+1}}. \tag{20}$$

A. Matrix elements

Having expressed the total interaction $U(r,\theta')$ (Coulomb + nuclear) in terms of the multipole expansion, Eq. (15), one can now easily calculate the diagonal as well as the off-diagonal couplings between states in the ground-state rotational band of ^{9}Be. All one needs to calculate is the matrix elements of the Legendre polynomials,

$$P_\lambda[\cos(\theta')] = \sum_\mu D_{\mu 0}^{\lambda *}(\hat{r}) D_{\mu 0}^{\lambda}(\mathbf{e}).$$

The matrix elements between different states are

$$\langle K I' M' | P_\lambda[\cos(\theta')] | K I M \rangle = \sqrt{\frac{2I+1}{2I'+1}} \sum_\mu D_{\mu 0}^{\lambda *}(\hat{r}) \langle I M \lambda \mu | I' M' \rangle \langle I K \lambda 0 | I' K \rangle. \tag{21}$$

The calculation is even simpler in the rotating frame approximation, which is used in the coupled-channels calculations described in the next section. In this approximation one assumes that **r** (the relative distance between projectile and target) defines the z axis. The angle θ' is then identical to the angle θ_e of the symmetry axis with respect to the z axis. Becausee $D_{\mu 0}^{\lambda}(\hat{z}) = \delta_{\mu 0}$, this implies that $\mu = 0$ is the only nonzero term in Eq. (21).

The total potentials one obtains for the two systems ^{9}Be + ^{144}Sm and ^{9}Be + ^{208}Pb are shown in Fig. 3. For each system the monopole potential (solid line) and the entrance channel potentials for the magnetic quantum numbers $m = 1/2$ and $3/2$ of the $3/2^-$, $K = 3/2$ ground state of ^{9}Be. All three potentials were obtained with the strength $v_r = 410$ MeV fm^3 of the repulsive effective NN interaction (which is determined in Sec. V A).

The magnetic quantum numbers $m = 1/2$ and $3/2$ used in Fig. 3 refer to a z axis that points in the direction of the relative position of projectile and target. The $m = 3/2$ channel therefore corresponds to an orientation where the tip of the deformed ^{9}Be points toward the target, whereas the $m = 1/2$ channel corresponds to the belly pointing toward the target. Consequently, the Coulomb barrier for the $m = 3/2$ entrance channel is lower than the barrier for $m = 1/2$.

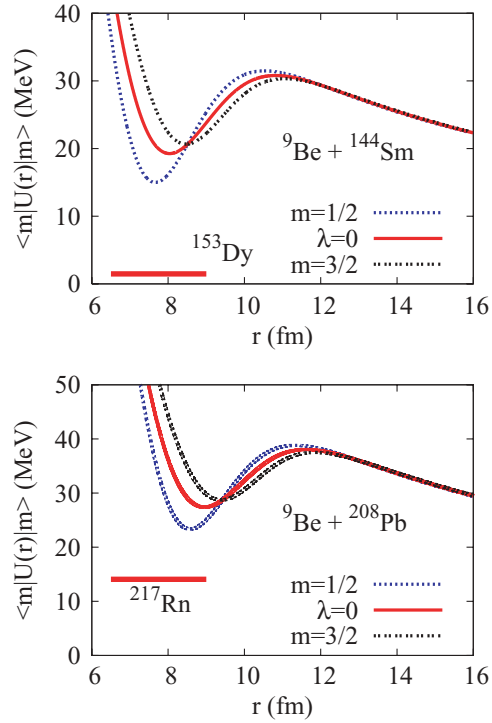

FIG. 3. (Color online) Entrance channel potentials for ^{9}Be + ^{144}Sm and ^{9}Be + ^{208}Pb, respectively, obtained for the repulsive strength $v_r = 410$ MeV fm^3. The solid (red) curve is the monopole potential; the dotted (blue and black) curves are the entrance channel potentials for the magnetic quantum numbers $m = 1/2$ and $3/2$. Ground-state energies of the two compound nuclei, ^{153}Dy and ^{217}Rn, are indicated.

Another observation is that the potential pocket is deeper for $m = 1/2$ than for $m = 3/2$. This is a consequence of the larger radius of curvature and the stronger nuclear attraction for the $m = 1/2$ belly configuration.

IV. MODEL OF ^{9}Be-INDUCED FUSION

The cross sections for the CF of ^{9}Be with a heavy target are calculated using the coupled-channels approach. CF is simulated by ingoing wave boundary conditions that are imposed in all channels at the minimum of the pocket in the entrance channel potential. Coupled equations are solved in the rotating frame approximation [17–19], where the z axis points in the direction of the separation vector **r** between the reacting nuclei. This approximation is also called the isocentrifugal approximation [17] because the centrifugal potential is the same in all channels and equal to the centrifugal potential in the entrance channel. The total magnetic quantum number m is also preserved in this approximation (see Ref. [20]). Because the ground state of the target is a 0^+ state and the ground state of ^{9}Be is a $3/2^-$ state, one would have to solve the coupled equations four times, for $m = \pm 1/2$ and $\pm 3/2$. For symmetry reasons it is actually sufficient to calculate the fusion cross section twice, for $m = 1/2$ and $3/2$, and compare the average fusion cross section with the data.

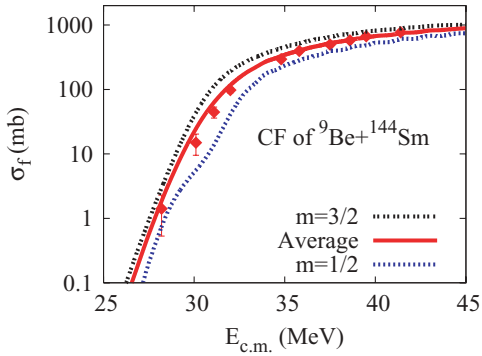

FIG. 4. (Color online) Measured cross sections for the complete fusion of $^{9}\mathrm{Be} + {}^{144}\mathrm{Sm}$ [3] are compared to calculations for $m = 1/2$ and $3/2$ and the average cross section [solid (red) curve]. The strength of the repulsive interaction was set to $v_r = 410$ MeV fm^3.

The effect of the decay of the excited state in ^{9}Be is included explicitly in the coupled equations by employing the complex excitation energies $E_I - \frac{i}{2}\Gamma_I$. The decay widths Γ_I are reported in the third column in Table I; it is seen that the width of the $7/2^-$ state is very large. The dominant decay mode of the $7/2^-$ state is neutron emission, and 55% of it populates the 2^+ excited state of ^{8}Be [8]. The latter state has an excitation energy of 3.03 MeV and a large width of 1.51 MeV, with an exclusive decay into two α particles [8]. The two α particles are emitted back to back in the ^{8}Be rest frame, so if one of them is emitted toward the target, the other α partner will recoil away from the target nucleus and will most likely escape. It is therefore assumed that the decay of the $7/2^-$ state will not lead to CF, and the CF will be calculated from the ingoing flux as described previously, whereas the decay is registered in the absorption cross section.

The data for the CF of $^{9}\mathrm{Be} + {}^{144}\mathrm{Sm}$ [3] are compared in Fig. 4 to the results of coupled-channels calculations. The calculated CF cross sections were derived from the ingoing flux as described previously. The top dotted curve is the cross section for the $m = 3/2$ magnetic substate; the lower dotted curve is for $m = 1/2$. The curve for $m = 3/2$ dominates the CF at all energies, consistent with the lower Coulomb barrier for this magnetic substate (see Fig. 3.) The data should be compared to the solid curve, which is the average of the CF cross sections for $m = 1/2$ and $3/2$. The comparison is discussed in more detail in Sec. V A.

A. Incomplete fusion

The decay of the $7/2^-$ state will end up in the breakup of ^{9}Be. The precise outcome of the decay in terms of ICF or breakup is not as clear. It would require a multicluster description to follow the two α particles after the decay. As mentioned earlier, it is unlikely that both α particles fuse with the target because they are emitted back to back. However, it is possible that one of them will fuse with the target nucleus and lead to ICF. It should also be emphasized that there are other sources of ICF, for example, neutron transfer from ^{9}Be, which are not included in the coupled-channels calculations presented here.

The calculated cross section for the decay of excited states is henceforth referred to as the absorption cross section. In view of the preceding discussion one should not expect that absorption would account for the measured ICF cross sections, but it is clearly of interest to compare the two cross sections. The experimental total fusion (TF) cross section is the sum of the CF and ICF cross sections. It is compared to the calculated TF cross section, which is the sum of the CF and the absorption cross sections.

V. COMPARISON TO MEASUREMENTS

The results of coupled-channels calculations that are based on the model presented in the previous sections are compared here to the data for CF and ICF of $^{9}\mathrm{Be} + {}^{208}\mathrm{Pb}$ [1,2] and $^{9}\mathrm{Be} + {}^{144}\mathrm{Sm}$ [3]. Both targets are spherical, closed-shell nuclei and the excitation of these nuclei is relatively weak compared to the excitation of ^{9}Be, so they will be ignored. Fusion with the ^{144}Sm target is discussed first because the couplings are weaker in this case and the adopted model is therefore expected to be more successful. This case will also provide the opportunity to calibrate the repulsive part of the effective NN interaction.

A. Fusion of $^{9}\mathrm{Be} + {}^{144}\mathrm{Sm}$

The calculated cross sections for the fusion of ^{9}Be with ^{144}Sm are compared in Fig. 5(A) to the data from Ref. [3]. The measured and calculated cross sections for CF are seen to be in good agreement. This was achieved by adjusting the repulsive part of the effective NN interaction that is used in the calculation of the double-folding nuclear potential. The best fit to the data is obtained for the strength $v_r \approx 410$ MeV fm^3, and that is the value that is used in the following. The χ^2 per data point is shown in Fig. 6 as a function of the strength of the repulsive interaction. There is another solution with a small χ^2 for $v_r \leqslant 300$ MeV fm^3 but it is unphysical because it produces a pocket for $^{9}\mathrm{Be} + {}^{208}\mathrm{Pb}$ that is deeper than the energy of the compound nucleus.

The dotted curve in Fig. 5(A) shows the calculated cross sections for the decay of the excited states of ^{9}Be; it is in surprisingly good agreement with the ICF data. The good agreement may be accidental but it could also indicate that the decay of the excited states of ^{9}Be is the main source of ICF for the ^{144}Sm target. The best fit to the data for TF is also achieved for $v_r \approx 410$ MeV fm^3. This consistency of the CF and TF is illustrated in Fig. 6 in terms of the χ^2 per data point.

The measured and calculated fusion cross sections are compared in a linear plot in Fig. 5(B). It is shown that the different components of the measured and calculated fusion cross sections are in good agreement. In particular, CF is suppressed by about 10% compared to TF at high energies, both experimentally and in the calculations. This suppression is caused in the coupled-channels calculations by the decay of the excited states of ^{9}Be. Without any decay in the coupled-channels calculations, the fusion cross section obtained from the ingoing-wave boundary conditions would be close to the measured TF cross section. In other words, the suppression of CF compared to TF requires some sort of

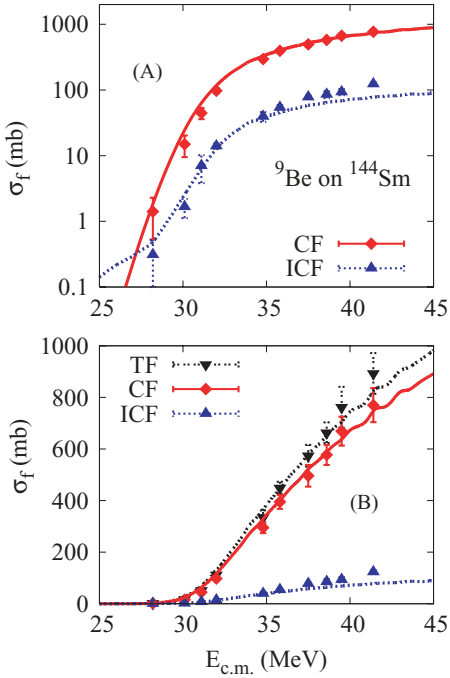

FIG. 5. (Color online) (A) Measured complete (CF) and incomplete (ICF) fusion cross sections for ^{9}Be + ^{144}Sm [3] are compared to calculated cross sections for CF [solid (red) curve] and absorption [dotted (blue) curve]. (B) This linear plot also shows the total fusion (TF) cross section.

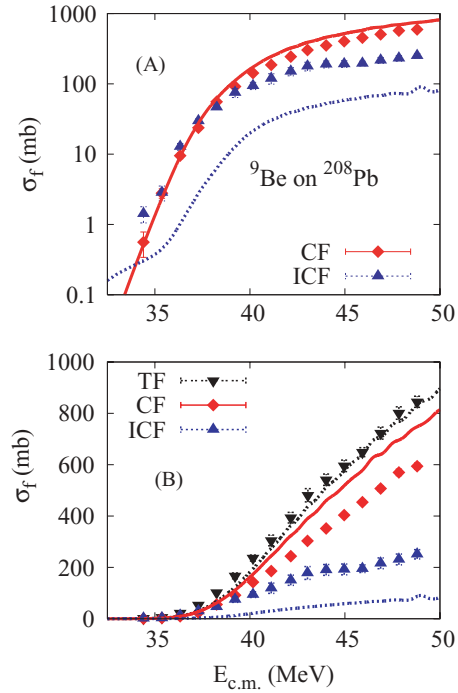

FIG. 7. (Color online) (A) Measured cross sections for complete (CF) and incomplete (ICF) fusion of ^{9}Be + ^{208}Pb [2] are compared to calculated cross sections for CF [solid (red) curve] and absorption [dotted (blue) curve]. (B) This linear plot also shows the total fusion (TF) cross sections.

absorption mechanism, and the decay mechanism suggested here seems to provide a natural explanation. Let us now investigate whether this mechanism can explain the data for the lead target.

B. Fusion of ^{9}Be + ^{208}Pb

The results of the coupled-channels calculations of the fusion of ^{9}Be + ^{208}Pb are compared in Fig. 7 to the data from Ref. [2]. The calculations are similar to those just presented for ^{9}Be + ^{144}Sm. It is shown in Fig. 7(B) that the calculated absorption cross section (owing to the decay of excited states) can only explain one-third of the measured ICF cross section at high energies. The suppression of the CF compared to the TF cross section is about 30% in the experiment [2], whereas the calculations show only a 10% suppression. There are evidently other sources of ICF in collisions of ^{9}Be with a ^{208}Pb target, besides the decay of excited states considered here.

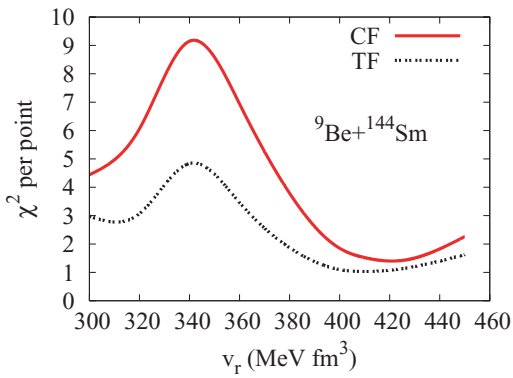

FIG. 6. (Color online) The χ^2 values per data point for complete (CF) and total (TF) fusion of ^{9}Be + ^{144}Sm are shown as functions of the strength v_r of the repulsive interaction, Eq. (17).

A 30% suppression of the CF data was observed in Ref. [2] by comparison to coupled-channels calculations. The calculations were based on a deformed Woods-Saxon potential but did not consider the effects of ICF or the decay of excited states. It was shown that a scaling of the calculated fusion cross section by a factor of 0.7 leads to a very good agreement with the CF data at all energies. In Fig. 7 it is sufficient to multiply the CF calculation by a factor of 0.8 to match the CF data at high energies. The reason for the smaller scaling factor is that the decay of the excited states has already taken care of a 10% reduction.

It is often necessary to employ a weak, short-range imaginary potential to be able to reproduce the fusion data of stable nuclei at high energies by coupled-channels calculations. This is particularly the case when calculations are based on a shallow entrance channel potential [10]. Because the potentials shown in Fig. 3 are relatively shallow, it is of interest to determine the effect of a weak imaginary potential on the fusion of ^{9}Be + ^{208}Pb. Let us therefore choose the potential

$$W(r) = W_0\{1 + \exp[(r - R_w)/a_w]\}^{-1}, \qquad (22)$$

with $a_w = 0.2$ fm and $R_w = 9.5$ fm, so that it acts near the minimum of the potential pockets shown in Fig. 3. The strength

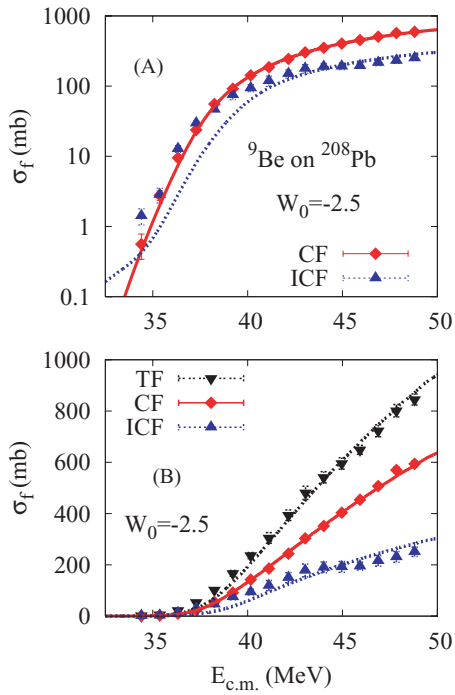

FIG. 8. (Color online) Similar to Fig. 7. Calculations include, in addition to the decay of the excited states of ^{9}Be, a weak imaginary potential with strength $W_0 = -2.5$ MeV.

W_0 was adjusted to optimize the fit to the CF data. The best fit is shown in Fig. 8(A); it was achieved for $W_0 = -2.5$ MeV and has a $\chi^2/N = 1.4$.

The absorption cross section, which is the combined effect of the imaginary potential, Eq. (22), and the decay of the excited states is shown by the lower dotted curves in Figs. 8(A) and 8(B). It is in good agreement with the ICF data at high energies, but the discrepancy is large at low energies. The discrepancy indicates that the breakup leading to ICF must take place at larger separations of projectile and target than assumed in the potential, Eq. (22). It may be possible to construct a more realistic imaginary potential (of the volume + surface type), but that idea is not pursued here.

There are other reaction channels that could be a source of ICF. Examples are the dissociation of ^{9}Be induced by neutron emission into the continuum and into bound states of the target nucleus. Both processes produce ^{8}Be that decays into two α particles, and one of them could end up as ICF. These reaction mechanisms should be studied theoretically in detail to develop a better understanding and description of the breakup, CF, and ICF. In fact, recent experiments [21] show that the ^{9}Be breakup following neutron transfer dominates the total breakup yield.

VI. CONCLUSIONS

The CF of ^{9}Be with spherical target nuclei was calculated using the coupled-channels approach. It was shown that the $B(E2)$ values for excitation of the ground-state rotational band of the ^{9}Be nucleus can be described quite well in the rotor model. This feature was exploited in the calculation of matrix elements of the interaction between the deformed projectile and a spherical target.

The interaction of the deformed ^{9}Be projectile with a spherical target was calculated using the double-folding technique and an effective M3Y NN interaction, which was supplemented with an adjustable repulsive term. The deformed density of ^{9}Be was determined so the measured quadrupole moment and rms charge radius were reproduced. The densities of the spherical targets were calibrated to reproduce the measured charge radii; the radius of the neutron density in ^{208}Pb was calibrated to be consistent with the neutron skin thickness predicted by Skyrme Hartree-Fock calculations and with the value extracted from measurements of antiprotonic ^{208}Pb atoms.

The double-folding potential was applied in coupled-channels calculations of the fusion of ^{9}Be with ^{144}Sm. The decay of the excited states of ^{9}Be was included explicitly in terms of complex excitation energies, whereas excitations of the target were ignored for simplicity. The repulsive part of the effective NN interaction, which essentially is the only parameter that remains to be determined, was adjusted to produce the optimum fit to the complete fusion data. The calculated cross sections for the decay of the excited states in ^{9}Be turned out to be in very good agreement with the ICF data.

Having determined all of the parameters of the theory, coupled-channels calculations were performed for the fusion of ^{9}Be + ^{208}Pb. At high energies the CF data were suppressed by 20% compared to the predicted cross sections, and the ICF data were a factor of 3 larger than the calculated cross section for the decay of excited states. There are obviously other reaction mechanisms, besides the decay of excited states, that are responsible for the large ICF cross sections that have been measured for the lead target. A likely candidate is the neutron transfer from ^{9}Be to bound states in the target and to continuum states. This is also the conclusion of a recent experimental investigation by Rafiei *et al.* [21].

ACKNOWLEDGMENTS

This work was supported by the US Department of Energy, Office of Nuclear Physics, under Contract No. DE-AC02-06CH11357.

[1] M. Dasgupta *et al.*, Phys. Rev. Lett. **82**, 1395 (1999).
[2] M. Dasgupta *et al.*, Phys. Rev. C **70**, 024606 (2004).
[3] P. R. S. Gomes *et al.*, Phys. Rev. C **73**, 064606 (2006).
[4] J. Randrup and J. S. Vaagen, Phys. Lett. B **77**, 170 (1978).
[5] Ş. Mişicu and W. Greiner, Phys. Rev. C **66**, 044606 (2002).
[6] Ş. Mişicu and W. Greiner, Phys. Rev. C **69**, 054601 (2004).
[7] A. Bohr and B. R. Mottelson, *Nuclear Structure*, Vol. II (Benjamin, New York, 1975).
[8] National Nuclear Data Center (BNL), Evaluated nuclear data structure files; http://www.nndc.bnl.gov/.
[9] D. R. Tilley *et al.*, Nucl. Phys. A **745**, 155 (2004).
[10] H. Esbensen and Ş. Mişicu, Phys. Rev. C **76**, 054609 (2007).

[11] H. de Vries, C. W. de Jager, and C. de Vries, At. Data Nucl. Data Tables **36**, 495 (1987).
[12] S. Yoshida and H. Sagawa, Phys. Rev. C **69**, 024318 (2004).
[13] B. Klos *et al.*, Phys. Rev. C **76**, 014311 (2007).
[14] R. B. Wiringa, S. C. Pieper, J. Carlson, and V. R. Pandharipande, Phys. Rev. C **62**, 014001 (2000).
[15] Ş. Mişicu and H. Esbensen, Phys. Rev. C **75**, 034606 (2007).
[16] E. Uegaki and Y. Abe, Prog. Theor. Phys. **90**, 615 (1993).
[17] J. Gomez-Comacho and R. Johnson, J. Phys. G **12**, L235 (1986).
[18] O. Tanimura, Phys. Rev. C **35**, 1600 (1987).
[19] H. Esbensen, S. Landowne, and C. Price, Phys. Rev. C **36**, 1216 (1987).
[20] H. Esbensen, Phys. Rev. C **68**, 034604 (2003).
[21] R. Rafiei, R. du Rietz, D. H. Luong, D. J. Hinde, M. Dasgupta, M. Evers, and A. Diaz-Torres, Phys. Rev. C **81**, 024601 (2010).